

APPLICATION OF THE THREE-DIMENSIONAL IMAGE EDGE FEATURE EXTRACTION IN MECHANICAL ARM POSITION GRASPING AND ATTITUDE DETECTION

Huihui Wu^{1*}, Xianrong Zeng¹, Yanjun Lai¹, Mingfeng Liang²

¹*School of Intelligent Manufacturing, Shunde Polytechnic, Foshan 528330, Guangdong, China;*

²*Eagle-eye Vision Intelligent Technology Company Limited, Foshan 528332, China.*

**Corresponding author: Huihui Wu*

Email: huihuiwu248@yeah.net

Abstract: In order to detect the position and attitude of the mechanical arm in the process of grasping, the kinematics model of the humanoid mechanical arm is established by using the screw theory. Based on the Monte Carlo method, the workspace point cloud image of the mechanical arm is obtained; the pixel coordinates of the image are extracted through the contour extraction algorithm of Halcon software. Combined with the hand-eye relationship, the position relationship between the camera and the mechanical arm base coordinate system is obtained. In the C++ environment, the secondary development of the mechanical arm is carried out to realize the basic functions of object positioning and robot control. Through the image analysis in MATLAB, it is observed that the extraction effect of workspace boundary points is good, and the curve fitting error is small, which lays the foundation for the follow-up trajectory planning and motion control of humanoid mechanical arm. Through real-time data monitoring and data initialization after each task, the problems of local optimization and convergence stagnation can be well solved, so that the image processing results that meet the requirements of mechanical arm self-recognition can be obtained, the iterative ergodic efficiency can be better improved, and the subsequent processing time can be shortened. The simulation results show that the algorithm can get better edge detection results. Finally, the robot can grasp the object. The application of three-dimensional image edge feature extraction technology makes the selection of objects faster and more accurate, which makes up for the shortcomings of traditional grasping technology. After this research, the application of three-dimensional image technology to further improve the mechanical arm's ability to grasp objects will gradually become widespread.

Keywords: Mechanical Arm; Three-Dimensional Image Detection; Monte Carlo Method; Contour Extraction Algorithm.

1. Introduction

The application field of robot is constantly expanding, and the concept is also constantly broadening, which is no longer limited to industrial robots for handling, welding and mass operation [1,2]. Robots are now widely used in various fields, and it is not in the era of novels or science fiction movies. With the great development of robot, as a very important key mechanism of robot, great progress has also been made on robot gripper [3]. As the last link and executive part of the interaction between robot and environment, robot arm is not only a perceptron that actively perceives the working environment information, but also a highly integrated electromechanical system with multiple sensing functions and intelligence, involving multiple

research fields and interdisciplinary subjects such as mechanism, bionics, and materials science [4,5]. Among them, the most important technology in mechanical arm grasping is edge detection, which is a basic problem in digital image processing and computer vision. Its purpose is to mark the points with obvious changes in various parameters in the image [6]. Edge refers to the external performance of the image due to the mutation of local characteristics [7]. Due to the significant changes of color, gray, texture and other data, the local image is discontinuous, so a certain standard can be used to calibrate the image segmentation boundary [8,9].

The edge detection method can provide more accurate position data for the robot to grasp the target image, which is the key step in the image processing process [10,11].

The use of three-dimensional image detection has greatly improved the progress of intelligence [12]. In the manufacturing industry, in order to improve the processing quality and production efficiency of products, it is necessary to carry out quality inspection on the production site. The three-dimensional quality detection of the workpiece can be realized through the three-dimensional restoration of the surface gray information of a single image [13,14]. Although there are many researches on three-dimensional shape restoration, most of them are still in the laboratory stage. Moreover, due to the limitations of accuracy, measurement range, working conditions and operation process, it is not easy to be applied to the automatic production line [15]. Among the existing three-dimensional shape restoration methods, the method based on shading is a simple and practical industrial on-line detection method. Based on the design idea of this method, the reflection model is improved by preprocessing the collected three-dimensional image and adding perspective projection constraints. Then, the industrial application in the field of three-dimensional inspection of workpiece surface is explored [16].

Therefore, the application of three-dimensional image detection technology to the mechanical arm will greatly ensure the accuracy and stability of the mechanical arm [17], which will be a big innovation for the work of traditional mechanical arm.

2. Research on Technology Module and Method

2.1 Working Principle of Intelligent Mechanical Arm System

Cameras are used to simulate the vision of robots. In this system, the camera is fixed to obtain the image of the object. After successful image acquisition of the object, the grey image threshold processing, high-pass filtering, edge extraction and other pre-processing are carried out; the single vision positioning is carried out. By acquiring the position of the object relative to the camera and the position of the camera relative to the mechanical arm, the position and attitude of the object relative to the mechanical arm are obtained, and the position and attitude of the object in the image are obtained.

$S_E(3)$ is a special Euclidean group; R is an attitude rotation matrix of order 3; t is a position vector; $S_E(3)$ is a subgroup of a lie group whose Lie algebra is $se(3)$, and the elements in $se(3)$ are defined as:

$$\xi = \begin{pmatrix} \sigma & v \\ 0 & 0 \end{pmatrix} \in \mathbb{R}^{4 \times 4} \quad (2)$$

In order to ensure the accuracy of position and attitude measurement, it is necessary to calibrate the internal and external parameters of the system, namely, camera calibration and hand-eye calibration, so that it can be converted in the world coordinate system, camera coordinate system, image coordinate system, and pixel coordinate system in sequence. After that, the position and attitude of the workpiece in the coordinate system of the mechanical arm are transmitted to the mechanical arm.

The contour extraction algorithm is used to extract the coordinate data of the object, which guides the mechanical arm to complete the workpiece grasping. Figure 1 shows the principle of its operation:

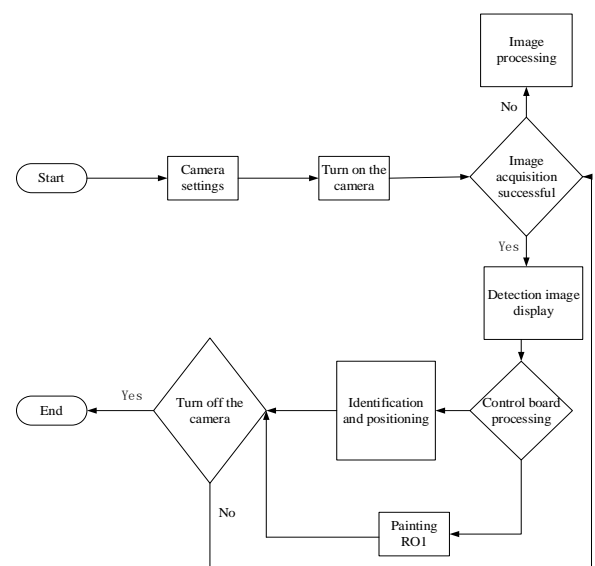


Figure 1: Working principle of mechanical arm

2.2 Screw Theory and Design of Mechanical Arm

a. Screw theory

In order to describe the position and attitude of a rigid body in space, two coordinate systems are established: the reference coordinate system $\{S\}$ and the object coordinate system fixed on the rigid body $\{T\}$. Then, the position and attitude of the rigid body relative to $\{S\}$ can be expressed by the relative pose of $\{T\}$ to $\{S\}$. All the corresponding position and attitude transformation matrices are expressed as follows:

$$S_E(3) = \left\{ \begin{pmatrix} R & t \\ 0 & 1 \end{pmatrix} \mid R \in \mathbb{R}^{3 \times 3}, t \in \mathbb{R}^3, R^T R = I, \det(R) = 1 \right\} \quad (1)$$

According to Chasles theorem, any rigid body motion can be realized by spiral motion, rotation around an axis and compound motion along the axis. The infinitesimal of spiral motion is Lie algebra, that is, the motion screw. There are two forms of motion screw.

$$\xi = \begin{pmatrix} \omega & v \\ 0 & 0 \end{pmatrix} \in \mathbb{R}^{4 \times 4}, \xi = \begin{pmatrix} \omega \\ v \end{pmatrix} \quad (3)$$

ω is the angular velocity of the rigid body around the axis; v is the linear velocity along the axis; ω is the antisymmetric matrix of ω .

According to the screw theory, the exponential coordinate form of motion screw can be used to represent the rigid body motion, that is, for any rigid body motion $g \in S_e(3)$, there is $g = e^{\xi\theta}$. The position and attitude transformation of the object coordinate system $\{T\}$ fixed on the rigid body relative to the reference coordinate system $\{S\}$ is represented by the rigid body motion ${}^S_T g(\theta)$. ${}^S_T g(0)$ is set as the initial pose of the object coordinate system in the reference coordinate system; after the spiral motion of the object coordinate system, the position and attitude relative to the reference coordinate system are as follows.

$${}^S_T g(\theta) = e^{\xi\theta} {}^S_T g(0) \quad (4)$$

b. Design of mechanical arm

The structure of the humanoid mechanical arm studied is similar to that of the human arm. The human arm can be regarded as a 3-link 7-DOF (degree of freedom) structure, that is, the main arm, forearm, palm 3 links and 3-DOF in shoulder, 1-DOF in elbow, three-DOF in wrist. With the reference of the structure of human arm, Figure 2 is the structure design of humanoid mechanical arm. The mechanical arm has 6-DOF. The difference from the human arm structure is that the wrist has 2-DOF. The above structural characteristics are the most significant characteristics of humanoid mechanical arm which are different from other types of mechanical arm.

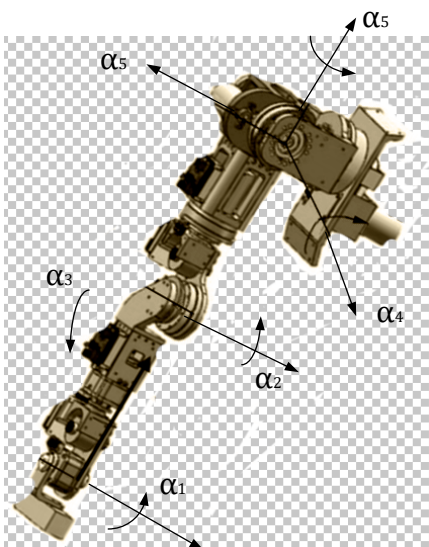


Figure 2: Mechanical arm model

According to the mechanical structure of humanoid mechanical arm and the motion of human arm, Table 1 is the definition and specific value of the mechanical arm parameters.

Table 1 Parameters of mechanical arm

Describe	Data	Result
Main arm L of mechanical arm	L1	260mm
Forearm L of mechanical arm	L2	258mm
Angle 1	α_1	$[-\pi/2, \pi]$
Angle 2	α_2	$[0, \pi]$
Angle 3	α_3	$[-\pi/2, \pi/2]$
Angle 4	α_4	$[0, 5\pi/6]$
Angle 5	α_5	$[-\pi/2, \pi/2]$
Angle 6	α_6	$[-\pi/2, \pi/2]$

c. Camera calibration

First, the internal and external parameters of the camera are calibrated. The internal parameters are mainly the basic matrix of the camera:

$$camera\ matrix = \begin{bmatrix} f_x & 0 & c_x \\ 0 & f_y & c_y \\ 0 & 0 & 1 \end{bmatrix} \quad (5)$$

and Distortion coefficients= $(k_1 k_2 p_1 p_2 k_3)$. The external parameters are mainly the rotation matrix of the camera:

$$R = \begin{bmatrix} \cos\theta\cos\alpha & \sin\theta\sin\alpha\cos\phi - \cos\theta\sin\phi & \cos\theta\sin\alpha\cos\phi + \sin\theta\sin\phi \\ \cos\theta\sin\alpha & \sin\theta\sin\alpha\sin\phi + \cos\theta\cos\phi & \cos\theta\sin\alpha\sin\phi - \sin\theta\cos\phi \\ -\sin\theta & \sin\theta\cos\alpha & \cos\theta\cos\alpha \end{bmatrix} \quad (6)$$

and the translation vector $T=[t_1,t_2,t_3]$. (x, y) are the physical coordinates of the image plane, and (X, Y, Z) are the actual world coordinates. Its relationship is that $x=M*$ the transformation of the physical coordinates of the object to the camera image. In the process of camera calibration, it is necessary to realize the transformation of world coordinate system, phase coordinate system, image coordinate system and pixel coordinate system in turn, and solve the error caused by the angle between the lens plane and the imaged plane due to the camera imaging sensor and installation position. Camera calibration coordinate system is mainly to collect data and parameters through computer vision technology, and then use computer technology to carry out three-dimensional modelling of

parameters, so as to restore the three-dimensional coordinates of the whole space. First, the camera is required to observe the calibration plate from different directions (at least two). After the image is loaded, the reference position and attitude are set and a projection map is created to describe the mapping between the image plane and the Z-zero plane in the coordinate axis system. The imaging principle of camera is pinhole imaging. Through mapping, the three-dimensional display world is transformed into two-dimensional image. Two-dimensional points are represented by $m=[u,v]^T$, and three-dimensional points by $M=[X,Y,Z]^T$. \tilde{x} denotes the augmented vector, and the last element plus 1: $\tilde{m}=[u,v,1]^T, \tilde{M}=[X,Y,1]^T$. The relationship between three-dimensional point M and its image projection point m is as follows.

$$sm = A[R \ t]M \quad \text{with} \quad A = \begin{bmatrix} \alpha & c & u_0 \\ 0 & \beta & v_0 \\ 0 & 0 & 1 \end{bmatrix} \quad (7)$$

s is an arbitrary scale factor. (R, t) is called external parameter, R is rotation matrix, and T is translation matrix. A is the camera internal parameter matrix, (u₀, v₀) is the main point of the coordinate, α and β are the scale factors of the image on the u and v axes, and c is the parameter describing the tilt angle of the two coordinate axes. If the Z coordinate of the model plane in the world coordinate system is zero, from the equation (8):

$$s \begin{bmatrix} u \\ v \\ 1 \end{bmatrix} = A \begin{bmatrix} r_1 & r_2 & r_3 \end{bmatrix} \begin{bmatrix} X \\ Y \\ 0 \\ 1 \end{bmatrix} = A \begin{bmatrix} r_1 & r_2 & r_3 \end{bmatrix} \begin{bmatrix} X \\ Y \\ 1 \end{bmatrix} \quad (8)$$

It can be seen that when Z=0, M can be expressed as $M = [X \ Y]^T$, and the same $\tilde{M} = [X \ Y \ 1]^T$. Therefore, the relation between the point M and its mapping point m in the image is connected by the identity matrix H.

The related matrix functions are obtained by using the constraint conditions of internal parameters:

$$H = [h_1 \ h_2 \ h_3][h_1 \ h_2 \ h_3] = \lambda A [r_1 \ r_2 \ t] \quad (9)$$

λ is an arbitrary scalar. Because r1 and r2 are orthogonal, it is concluded that:

$$\begin{aligned} h_1^T A^{-T} A^{-1} h_2 &= 0 \\ h_1^T A^{-T} A^{-1} h_1 &= h_2^T A^{-T} A^{-1} h_2 \end{aligned} \quad (10)$$

According to this matrix, the closed solution is obtained.

The above is obtained by minimizing the algebraic distance, so it needs to be improved by using the maximum likelihood estimation. Maximum likelihood estimation can be obtained by finding the minimum value of the following function.

$$\sum_{i=1}^n \sum_{j=1}^m \|m_{ij} - m(A, R_i, t_i, M_j)\|^2 \quad (11)$$

The radial distortion produced by camera lens also needs to be processed. First, the coordinates of the centre point of the image are input, and then the main point of the corrected image is obtained by Zhang's calibration method. The width to height scaling ratio of the output image and the corrected image is calculated and mapped to the corrected image coordinates, and the coordinates are mapped to the input image coordinates by Zhang's calibration method. Then, bilinear interpolation is used to optimize the algorithm. The centre of the source image and the target image is aligned, and the floating-point operation is converted into integer operation.

2.3 Spatial Image Processing

a. Image processing

Image processing is an important part in the process of vision guided robot motion. Only by making the robot accurately obtain the shape features of the target image, can the robot move correctly. In this system, Halcon is used to transform the grey level into RGB three channels and then HSV channel, so as to select the selected area better;

After that, the coarse positioning is carried out, and the image is processed once to roughly find out the positioning area, select the appropriate channel, and carry out threshold processing in the grey histogram; then, the fine positioning is carried out, and the ROI area is generally drawn to perform the secondary processing; the threshold processing is carried out again to accurately determine the selected area; the connected domain is made, the appropriate structural elements are created, and the expansion and opening operation are carried out to get A images; according to the feature histogram, multiple feature values are obtained, and the accurate recognition area is determined to get the image B; the intersection of AB is taken to get the image C; finally, the image C is denoised to provide information for the subsequent robot grasping work. After the completion of image processing, hand-eye calibration is performed on the object. What the camera knows is the pixel coordinate, and the mechanical arm is the spatial coordinate system, so the hand-eye calibration is to get the coordinate transformation relationship between the pixel coordinate system and the spatial mechanical arm coordinate system.

In the actual control, after the camera acquires the pixel position of the object in the image, the pixel coordinates of the camera are transformed into the spatial coordinate system of the mechanical arm through the calibrated coordinate transformation matrix, and then how each motor should move is calculated according to the mechanical arm coordinate system, so as to control the mechanical arm to reach the specified position.

b. Solution of mechanical arm workspace

The workspace of mechanical arm includes total workspace and flexible workspace. The total workspace is the area of all the position points that the end reference point of the mechanical arm can reach, and the flexible workspace is the area of all the position points that the mechanical arm can reach through a variety of postures. The total workspace of the reference point on the end of the humanoid mechanical arm is analyzed. Due to the limitation of structural parameters and joint angle range, the workspace of the mechanical arm will be limited accordingly.

According to the forward kinematics modelling, the workspace of the mechanical arm can be expressed as:

$$P = \{(P_x, P_y, P_z)\} \tag{12}$$

Monte Carlo method is a numerical method to solve mathematical problems with the help of random sampling. This method has fast calculation speed and is suitable for workspace analysis of various joint manipulators. In MATLAB, the specific steps of obtaining mechanical arm workspace by Monte Carlo method are as follows:

(1) The forward kinematics equation of the humanoid mechanical arm is solved to obtain the position vectors (P_x, P_y, P_z) of the end reference point in the reference coordinate system, as shown in equation (12).

(2) Random function rand is used to generate random values of joint variables.

$$\alpha_i = \alpha_{i_{min}} + (\alpha_{i_{max}} - \alpha_{i_{min}}) * rand(N, 1) \tag{13}$$

N is the number of random points; θ_{imax} and θ_{imin} are the upper and lower limits of joint variables; i is the number of joints, taking $1 \sim 6$.

$$\begin{cases} f_1 = a_1\alpha + a_2, (\pi/2 \leq \alpha < 3\pi/2) \\ f_2 = b_1\alpha^4 + b_2\alpha^3 + b_3\alpha^2 + b_4\alpha^1 + b_5, (0 \leq \alpha < \pi/2) \\ f_3 = c_1\alpha^5 + c_2\alpha^4 + c_3\alpha^3 + c_4\alpha^2 + c_5\alpha^1 + c_6, (3\pi/2 \leq \alpha < 2\pi) \end{cases} \tag{16}$$

a_1 and a_2 are 0.2131 and 513.3643, respectively; $b_1 \sim b_5$ are 24.9121, -279.1148, -544.9525, -68.4695 and 202.7651, respectively; $c_1 \sim c_6$ are 148.1615, -

(3) The random values of N groups of joint variables are introduced into equation (13), so that the position coordinates of the reference point at the end of the mechanical arm are obtained.

(4) The position coordinates of the reference points are described to obtain the workspace of the humanoid mechanical arm. The larger the number of random points N is, the higher the calculation accuracy of the workspace is, and the closer the workspace is to the actual workspace. When $N=500000$, the workspace point cloud of humanoid mechanical arm can be obtained

2.4 Boundary Curve Fitting

The workspace boundary of humanoid mechanical arm is generally smooth, so the ordinary least squares are used to fit the extracted workspace boundary points. The ordinary least squares make the sum of square error minimum, search the optimal curve function, obtain the function expression of smooth boundary curve, and calculate the size of workspace. First, the boundary points (x_i, y_i) of each layer are transformed from Cartesian coordinates to polar coordinates (P_i, α_i) . The conversion relationship is:

$$\begin{cases} p = \sqrt{x^2 + y^2} \\ \alpha = \arctan \frac{y}{x} \end{cases} \tag{14}$$

Then, the ordinary least squares are used to fit the boundary points. The coordinate function of the internal and external boundary is $f = P(\theta)$, and the sum of error square sum E^2 is the minimum, that is,

$$E^2 = \sum [p(\alpha_i) \sin \alpha_i - y_i]^2 \tag{15}$$

The characteristics, fitting effect and computational complexity of boundary curve are considered comprehensively.

The piecewise polynomial function is used to fit the outer boundary points. By combining the outer boundary points of x-y plane workspace, the polynomial function expression is obtained as follows.

545.3092, 488.0462, 128.8918, 6.2287 and 199.8445, respectively.

The boundary point fitting curve of x-y plane workspace. When the ordinary least squares are used to fit the boundary points, the curve is smooth and the fitting error is small. The area between the outer circle curve and the inner circle curve is the workspace of the humanoid mechanical arm in this plane.

3. Simulation Results and Image Analysis

3.1 Simulation Mechanical Arm

Figure 3 shows the space diagram of the two mechanical arms:

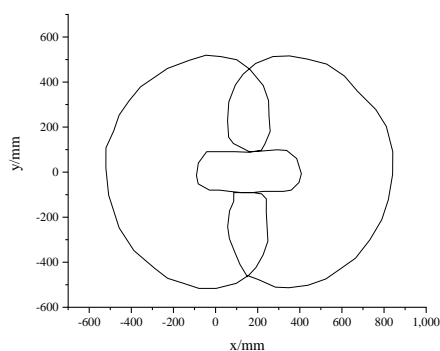


Figure 3: Planar workspaces of two mechanical arms

Based on the workspace analysis of a single humanoid mechanical arm, the cooperative workspace of two humanoid mechanical arms is obtained, and then the cooperative work of the two arms is analyzed briefly. Here, the more common two arm cooperative work to carry objects is taken as an example.

The solution process of the workspace of the two humanoid mechanical arms is similar to that of the single arm, so it is easy to get the workspace point cloud of the two arms. The intersection area of spatial point cloud is the cooperative workspace of two arms. As can be seen from the previous text, Figure 3 shows the two arms cooperative workspace on the x-y plane. In addition to the rectangle, the shadow area is the two arms cooperative workspace on the plane, that is, the two arms cooperative work can be carried out in this area.

The rectangular shadow area is approximately the area of the two arms body. Before objects are moved, it is necessary to determine whether the object is in the two arms cooperative workspace.

Figure 4 is the space image rendering of the mechanical arm.

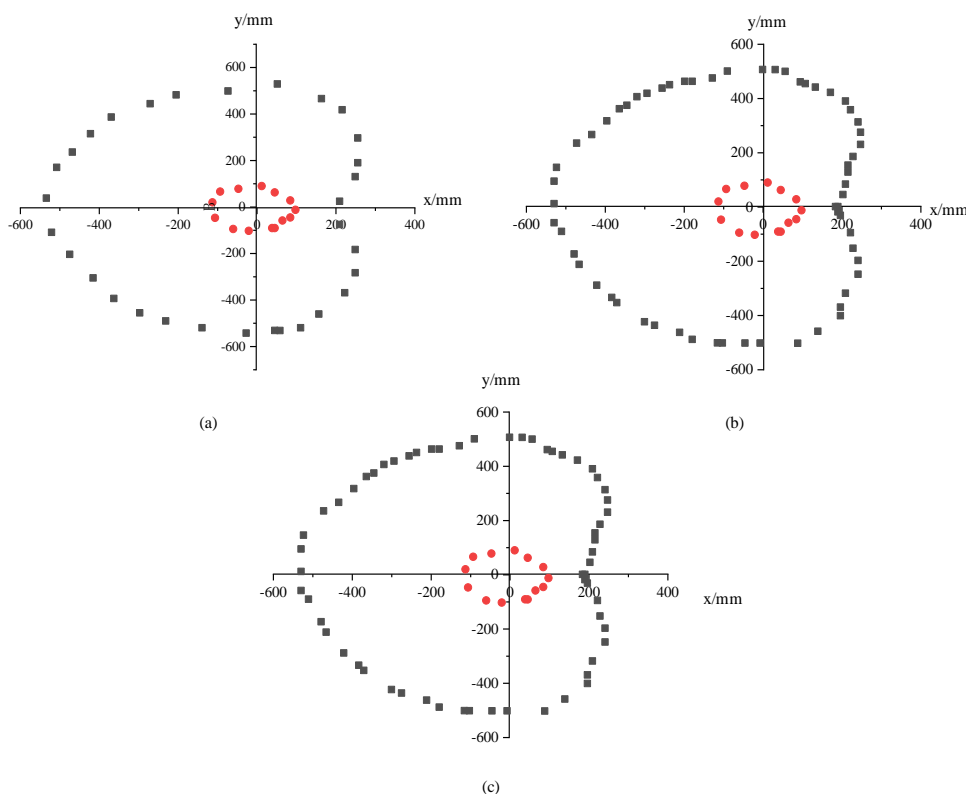


Figure 4: The effect of MATLAB boundary points (a: plane boundary point graph, b: pseudo boundary point graph, c: eliminating pseudo boundary point)

The number of random points is $N=12000000$. The workspace is divided into 25 layers along the Z-

axis, and each layer is divided into 120 fan-shaped areas, as shown in Figure 4. Figure 4(a) shows that

the circle formed by the points on the inner ring is the inner boundary of the workspace, indicating that there is a cavity in the workspace, and its size is affected by the length of the mechanical arm and the range of joint angle. Figure 4(a) is the whole workspace of the humanoid mechanical arm. It suggests that the extracted boundary points have good uniformity. There may be a few "pseudo boundary points" in the extracted inner and outer boundary points, such as the point W shown in Figure 4(b). The existence of "pseudo boundary points" will affect the extraction accuracy of boundary points.

The more the number of "pseudo boundary points" is, the lower the fitting accuracy of boundary curve is.

The method of distance comparison between points is used to eliminate the "pseudo boundary points" in boundary points. First, the distance between each point in the inner and outer boundary points and its adjacent points is calculated respectively; then, the calculated two distance values are compared with the set threshold value. If at least one distance value exceeds the threshold, the point is judged as "pseudo boundary point". Figure 4(c) shows the effect of eliminating "pseudo boundary points" by this method. It reveals that this method can eliminate "pseudo boundary points" better.

As shown in Figure 5, the simulation workspace shows that the humanoid mechanical arm can realize the motion function of human arm.

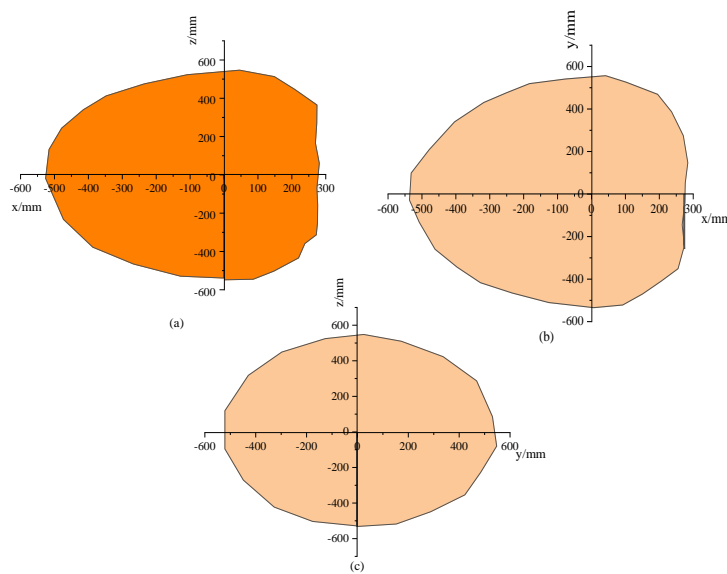


Figure 5: Three-dimensional workspace diagram of MATLAB simulation mechanical arm (a: X-Z direction B: X-Y direction C: Y-Z direction)

3.2 Grab Test Results of Mechanical Arm

After camera calibration, image processing and calibration, the accurate position of the object is

obtained. At this time, it is necessary to guide the robot to grasp the object.

Figure 6 is a graph of the claw position of the mechanical arm.

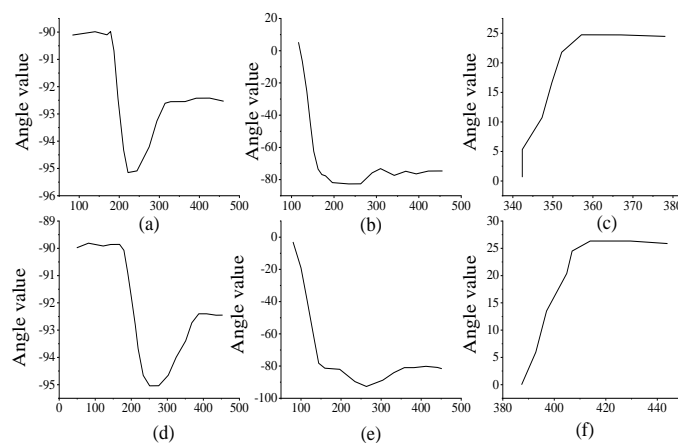


Figure 6 Movement angle curve of mechanical arm's claw (a-f is the rotation angle value change curve of joint 1-6)

The program of image acquisition and processing in Halcon is exported and transformed into C++ format, and then the program is opened in VS2010. At this point, the program is divided into three parts. The first part is the function declaration part, the second part is the function program part, and the third part is the whole function call part. The operators used in the Halcon internal editing of the three parts of the program become encapsulated functions after they are exported into C++ programs. In order to make the mechanical arm grasp the required objects in the secondary development, this system uses the SDK development kit to develop on the C++ development platform. The SDK package is imported into the new C++ project, the header file is added, the network is initialized, and the instantiation of the mechanical arm is obtained. The mechanical arm connection is waited for, the mechanical arm is initialized and unlocked, and its length is set to make it moves to grab the desired object. Every time in the process of grabbing, the data will be initialized to ensure the success rate of grabbing results.

4. Discussion

Camera is equivalent to the "eye" of an object. It can be used to collect objects in real time and accurately locate the three-dimensional images. The problem of robot capturing the target object in case of the change of external environment can be solved. For an object, a series of operations such as position and attitude measurement, camera calibration, hand-eye calibration, image processing, and transferring the position and attitude to the mechanical arm are carried out to guide the mechanical arm to grasp the object [18,19]. In this process, some system errors and random errors will appear. It is necessary to perform continuous optimization, and reduce system error and random error until near the ideal target.

Monte Carlo method is used to get the workspace point cloud of the mechanical arm. After the three-dimensional point cloud is layered, the inner and outer boundary points of the workspace are extracted by combining the angle division method and the two-parameter arctangent function. In view of the possible existence of "pseudo boundary points", the distance comparison method between points is used to eliminate "pseudo boundary points" [20]. MATLAB simulation results show that the extracted workspace boundary points have good uniformity. The ordinary least squares are used to fit the piecewise polynomial curve of the boundary point of the workspace, and the boundary curve of the workspace is obtained. The fitting curve is smooth and the fitting error is small. The cooperative workspace of two humanoid mechanical arms is analyzed briefly.

With moving objects as an example, it shows that workspace analysis has a certain guiding role in the designated trajectory planning [21,22].

5. Conclusion

Through the three-dimensional image edge feature extraction technology, the mechanical arm does not need manual adjustment in grasping objects, which is easy to operate and suitable for image pre-processing stage with wide adaptability and good effect. Compared with the previous intelligent extraction technology, it can extract objects with different structures more comprehensively. In addition, the MATLAB simulation analysis of the image captured by the mechanical arm clearly reveals that the mechanical arm's grasp of the object position is quite stable, which also reflects the advantage of the contour extraction algorithm in the application of image feature capture of the mechanical arm.

However, for the object with too large volume, because of the limitations of the camera, it is impossible to extract the complete position data of the object, which may lead to the failure of capture. At the same time, in different environments, such as dark, reflective and other harsh conditions, the camera function will lose its accuracy, which will lead to the failure of the capture function. Now, it can only be applied to some normal environment extraction, so choosing a better detector that can adapt to various environments is the main direction of the device improvement.

Acknowledgment

This work was supported by Characteristic innovation projects of scientific research in Guangdong Universities in 2020 (2020KTSX365).

References

- [1] Zhang C.Y. (2020) PD Plus Dynamic Pressure Feedback Control for a Direct Drive Stewart Manipulator. *Energies*, 13(5), 607.
- [2] Zhang D. J., Zhang G. Y., Li L. Q. (2019) Calibration of a six-axis parallel manipulator based on BP neural network. *The Industrial Robot*, 46(5), 692-698.
- [3] Reza Z., Saeed K. (2019) Direct adaptive model-free control of a class of uncertain nonlinear systems using Legendre polynomials. *Transactions of the Institute of Measurement and Control*, 41(11), 3081-3091.

- [4] Zhou Z. Y., Wang C., Zhu Z. F., et al. (2019) Sliding mode control based on a hybrid grey-wolf-optimized extreme learning machine for robot manipulators. *Optik*, 185, 364-380.
- [5] Ammar Z., Mohamed K., Ahmed T., et al. (2018) A new robust observer design for nonlinear systems with application to fault diagnosis. *Transactions of the Institute of Measurement and Control*, 40(13), 3696-3708.
- [6] Begnini M., Bertol B. W., Martins N. A. (2017) A robust adaptive fuzzy variable structure tracking control for the wheeled mobile robot: Simulation and experimental results. *Control Engineering Practice*, 64, 27-43.
- [7] Zhang A., Lai X. Z., Wu M., et al. (2017) Nonlinear stabilizing control for a class of underactuated mechanical systems with multi degree of freedoms. *Nonlinear Dynamics*, 89(3), 2241-2253.
- [8] Neuschwander K., Moll J., Memmolo V., et al. (2019) Simultaneous load and structural monitoring of a carbon fiber rudder stock: Experimental results from a quasi-static tensile test. *Journal of Intelligent Material Systems and Structures*, 30(2), 272-282.
- [9] Ullah M. I., Ajwad S. A., Irfan M., et al. (2016) Non-linear Control Law for Articulated Serial Manipulators: Simulation Augmented with Hardware Implementation. *Elektronika ir Elektrotechnika*, 22(1), 3-7.
- [10] Kapoor N., Ohri J. (2016) Fuzzified PSO-SVM controller for motion control of robotic manipulator. *Int. J. of Industrial and Systems Engineering*, 24(3), 361-383.
- [11] Nandhakumar S., Muthukumaran V., Soorya P. K. (2015) Position control of industrial robotic manipulator using variable structure control system with single term Haar wavelet series method. *Journal of Vibration and Control*, 21(12), 2465-2483.
- [12] Sun T., Liang G., Li X. D., et al. (2021) RobotDrlSim: A Real Time Robot Simulation Platform for Reinforcement Learning and Human Interactive Demonstration Learning. *Journal of Physics: Conference Series*, 1746(1), 012035.
- [13] Moon D. H., Shin S. H., Na J. B., et al. (2020) Fluid-Structure Interaction Based on Meshless Local Petrov-Galerkin Method for Worm Soft Robot Analysis. *International Journal of Precision Engineering and Manufacturing-Green Technology*, 7(9), 727-742.
- [14] Ozakyol H., Karaman H., Bingul Z. (2019) Advanced robotics analysis toolbox for kinematic and dynamic design and analysis of high-DOF redundant serial manipulators. *Computer Applications in Engineering Education*, 27(6), 1429-1452.
- [15] Zhao X.J., Chung Y. C. (2019) Development of a Robotic Structural Steel Cutting System. *IOP Conference Series: Materials Science and Engineering*, 538(1), 012042.
- [16] Korea J. (2019) Institute of Information, Electronics, and Communication Technology, 12(2). 170-177.
- [17] Koca G. O., Dogan S. (2019) ThreeDimensional Searching Surface Path Planning of Mobil Robots. *Bitlis Eren Üniversitesi Fen Bilimleri Dergisi*, (1), 298-307.
- [18] Kristensen C. B., Sørensen F. A., Nielsen H. B. (2019) Towards a Robot Simulation Framework for E-waste Disassembly Using Reinforcement Learning. *Procedia Manufacturing*, 38, 225-232.
- [19] Abe S., Noguchi N., Matsuka Y. (2018) Educational effects using a robot patient simulation system for development of clinical attitude. *European Journal of Dental Education*, 22(3), e327-e336.
- [20] Sangdani M. H., Saleh A. R. (2018) Genetic algorithm-based optimal computed torque control of a vision-based tracker robot: Simulation and experiment. *Engineering Applications of Artificial Intelligence*, 67, 24-38.
- [21] Supsomboon S., Varodhomwathana T. (2017) Robot and Plant Simulation for Automotive Part Production Process Design: A Case Study. *International Journal of Simulation Modelling*, 16(4), 617-629.
- [22] Sütő S., Forgó Z., Roşca F. T. (2017) Simulation Based Human-robot Co-working. *Procedia Engineering*, 181, 503-508.